Metabolic profiling reveals disorder of amino acid metabolism in four brain regions from a rat model of chronic unpredictable mild stress

By: Yan Ni, Mingming Su, Jinchao Lin, Xiaoyan Wang, Yunping Qiu, Aihua Zhao, Tianlu Chen and Wei Jia

Ni, Y., Su, M., Lin, J., Wang, X., Qiu, Y., Zhao, A., Chen, T., Jia, W. (2008) Metabolic profiling reveals disorder of amino acid metabolism in various brain regions from a rat model of chronic unpredictable mild stress, FEBS Letters. 582 (17): 2627-2636. doi:10.1016/j.febslet.2008.06.040

Abstract:

Chronic stress is closely linked to clinical depression, which could be assessed by a chronic unpredictable mild stress (CUMS) animal model. We present here a GC/MS-based metabolic profiling approach to investigate neurochemical changes in the cerebral cortex, hippocampus, thalamus, and remaining brain tissues. Multi-criteria assessment for multivariate statistics could identify differential metabolites between the CUMS-model rats versus the healthy controls. This study demonstrates that the significantly perturbed metabolites mainly involving amino acids play an indispensable role in regulating neural activity in the brain. Therefore, results obtained from such metabolic profiling strategy potentially provide a unique perspective on molecular mechanisms of chronic stress.

Keywords: Chronic unpredictable mild stress; Metabolic profiling; GC/MS; Multi-criteria assessment; Multivariate statistics; Amino acid

Abbreviations: NMR, nuclear magnetic resonance; MS, mass spectrometry; GC/MS, gas chromatography/mass spectrometry; PCA, principal component analysis; OPLS-DA, orthogonal partial least squares project to latent structures-discriminant analysis; MCA, multi-criteria assessment; VIP, variable importance in the projection; CUMS, chronic unpredictable mild stress; SNS, sympathetic nervous system; CNS, central nervous systems; HPA, hypothalamic–pituitary–adrenocortical; ECF, ethyl chloroformate; $CIJF_{jk}$, jack-knifed confidence interval; NAA, *N*-acetyl aspartate; BCAAs, branched-chain amino acids

Article:

1. Introduction

Depression is a serious public mental but treatable problem, affecting about 12% of women and 7% of men annually in USA [1]. It interferes often with normal feelings and behavior in people's daily life, and causes severe psychological pain for the patients and their families. Current treatments for clinical depression commonly involve psychotherapy and antidepressant medications. The most popular types of these antidepressant drugs are selective serotonin reuptake inhibitors (SSRIs), e.g., fluoxetine, citalopram, sertraline and several others [2].

Chronic unpredictable mild stress (CUMS), a well-validated animal model, has been used widely for studying clinical depression as well as evaluating antidepressant effects of diverse drugs [3]

and [4]. Much of the work has been done successfully in individual gene expression, protein structure and function, as well as biochemical studies on sympathetic nervous system (SNS), hypothalamic–pituitary–adrenocortical (HPA)-axis, noradrenergic and immunological systems, etc. [5], [6], [7], [8], [9] and [10]. Recently, the emerging metabonomics or metabolomics [11] and [12] has gradually studied the intricate relationship between acute and/or chronic stress and certain crucial endogenous metabolites [13], [14], [15], [16] and [17]. Such metabolic profiling technology has been increasingly used as a versatile tool for the discovery of molecular biomarkers in many areas such as monitoring the chemical-induced toxicity in organs, diagnosing or prognosing clinical diseases, exploring the potential mechanism of diverse diseases, and assessing therapeutic effects of drugs [18], [19], [20] and [21]. Relying on the global metabolite changes in a given biological species, metabol/nomics requires little or no prior knowledge on a certain disease. Thus, it potentially provides not only a means of verifying the fragmentary findings from a great deal of individual previous research, but also a promising opportunity to generate novel hypothesis for addressing the molecular mechanisms of diseases, ultimately towards a comprehensive understanding of physiopathological outcomes of an organism in response to xenobiotic stimuli and/ or genetic modification.

Biofuilds such as urine and plasma have been heavily used in metabol/nomic studies because they are minimally invasive to the animals or human and primarily reveal an overall metabolic state of the given organism [22]. By comparison, the tissue samples can offer a unique perspective on localized metabolic information. As the brain is a highly complex system encompassing a broad array of mutually interacting metabolites with varied chemical properties and specific biological functions, metabolic profiling of brain tissue samples will yield beneficial knowledge most related to neural activity of central nervous systems (CNS) [23], [24] and [25]. Yet no such study has been fully initiated to monitor neurochemical changes in a CUMS model.

Recent metabolic profiling technology has successfully applied high-throughput analytical tools (e.g., NMR, nuclear magnetic resonance; MS, mass spectrometry) to analyze various biological samples and utilized multivariate statistics (e.g., PCA, principal component analysis; PLS, partial least squares projection to latent structures) to extract meaningful biological information from the resultant complex and huge data sets [26 and [27]. Variable selection is an important step in multivariate analysis that can apparently enhance our understanding and interpretability of multivariate models and commonly referred to VIP statistics, loading weights, and correlation coefficients [28], [29] and [30]. However, the practical use of these methods relies mostly on the experimental designs and purposes (e.g., animal or human studies, biomarker identification or pathway analysis), the size of samples, and preference of researchers as well [31] and [32]. A strict approach for selecting significant and reliable variables should likely be a combination of multiple criteria. For instance, the newly proposed S-plot combines both covariance and correlation deriving from multivariate modeling [31]. But the exact criterion for each method in variable selection is hitherto not addressed thoroughly.

The primary goal of this work is to characterize neurochemical abnormalities in four discrete brain regions including cerebral cortex, hippocampus, thalamus, and the remaining regions from a rat model of CUMS. We applied a gas chromatography/mass spectrometry (GC/MS) technique to profile the brain tissue samples, and multi-criteria assessment (MCA) for multivariate statistics to select reliable variables accountable for class discrimination of metabolic profiles.

The differential metabolites were verified partially by qualitative and quantitative analyses simultaneously. This work will not only provide a constructive protocol in choosing the most reliable and significant metabolites associated with a certain pathophysiological state when using metabolic profiling technology, but also expand our understanding of molecular mechanisms for diverse diseases.

2. Materials and methods

The schematic flowchart of the metabolic profiling strategy used in this study is illustrated in the Fig. 1.

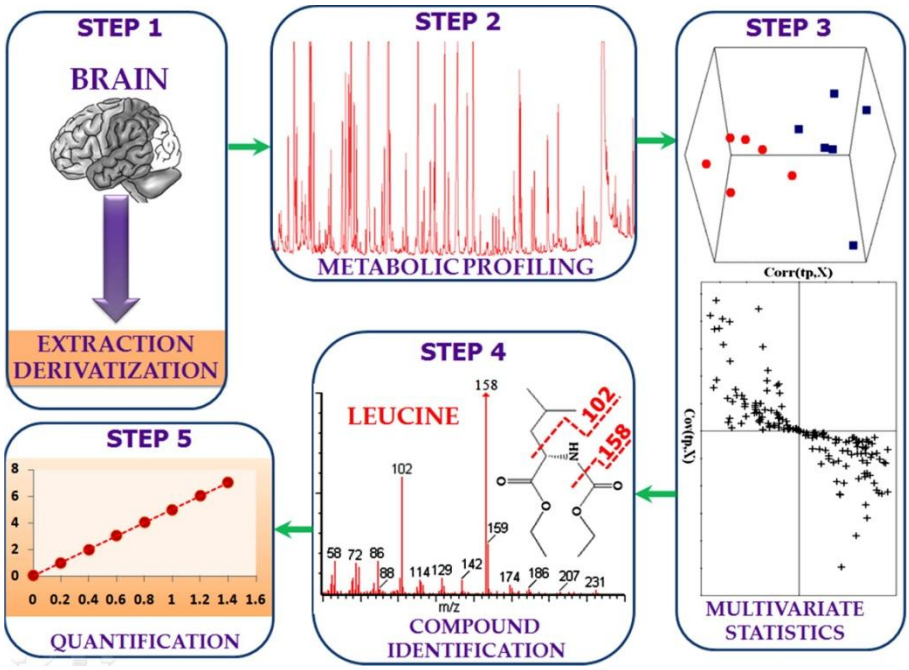

Fig. 1. Schematic flowchart of the metabolic profiling strategy used in this study. The homogenized tissue samples were extracted using ultrapure water and derivatized with ethyl chloroformate (ECF) (Step 1). The resultant derivatives were subsequently analyzed by a hyphenated technique – gas chromatography/mass spectrometry (GC/MS) (Step 2). Multivariate statistics was applied to extract meaningful information in the complex GC/MS spectral data (Step 3). Compounds with significant contribution to the variation of metabolic profiles between the CUMS-induced rats and healthy controls were identified in discrete brain regions using GC/MS spectral libraries including Wiley, NIST, NBS, etc., and further verified by reference compounds available (Step 4). Quantitative analysis of these verified metabolites was finally conducted by means of conventional calibration curves in order to accurately determine the concentrations of these metabolites in each brain region (Step 5).

2.1. Animal handling, sampling and sucrose preference test

The study was approved by national legislations of China and local guidelines. A total of twelve eight-week-old male Sprague–Dawley (SD) rats (n = 6 *per* group) was employed in this study and the animal experiment is described in the Supporting Materials.

2.2. Sample preparation, GC/MS assay, and data acquisition and pretreatment

The section was conducted as our previously described procedures [33] and is provided in the Supporting Materials.

2.3. Multivariate and univariate statistics

Multivariate statistics, including unsupervised PCA and supervised orthogonal partial least squares project to latent structures-discriminant analysis (OPLS-DA), was performed by SIMCA-P 11.0 software (Umetrics, Umeå, Sweden) [34] and [35]. The data set was mean-centered and pareto-scaled in a columnwise manner for all the multivariate modeling [36]. Mean centering calculates the average spectrum of the data set and subtracts that average from each spectrum, aiming to focus on the fluctuating part of data instead of the original value. Pareto scaling weighs each variable by the square root of its standard deviation, which amplifies the contribution of lower concentration metabolites but not to such an extent where noise produces a large contribution. PCA technique was initially used to reduce the high dimensional data sets into a two- or three-dimensional scores map without losing profound information. The resulting PCA scores map was used for investigating natural interrelation including possible groupings, clustering, and outliers among observations.

Furthermore, a more sophisticated OPLS-DA model was achieved through removing the variation in **X** matrix unrelated to **Y** matrix so that the specific discriminant information between classes can be interpreted using one predictive component alone [34] and [37]. Great efforts have been made to test the reliability of multivariate models [38] and [39], hence the 6-round cross-validation in SMICA-P software was herein applied to validate the OPLS-DA model against over-fitting by precluding 1/6th of all the samples in each round. The cross-validated OPLS-DA scores map depicts the between-class separation (t_p) and predictive ability ($Q^2\mathbf{Y}$) simultaneously [32]. Each individual in this map is represented by two spatial dots: one for model score value (t_p) and the other for cross-validated score value (t_{cv}). A smaller difference between the two score values suggests a better predictive accuracy ($Q^2\mathbf{Y}$).

Additionally, unpaired student's *t*-test implemented in Microsoft Office Excel 2007 (Microsoft (China) Co., Ltd. Beijing, China) was used to determine if the discriminant score values or the concentrations of the differential metabolites obtained from OPLS-DA modeling are statistically significant between classes at a univariate analysis level. The threshold of *P* value was set at 0.05 throughout the study.

2.4. Variable selection in OPLS-DA model

The main purpose and procedure of variable selection is illustrated in the Fig. 2. Variable importance in the projection (VIP) ranks the overall contribution of each variable to the OPLS-DA model, and those variables with VIP > 1.0 are considered statistically significant in this model. Herein, VIP statistics was initially applied to obtain the significant variables that could be used for metabolic pathway analysis [30]. Furthermore, MCA was used for choosing the most significant and reliable variables using a combination of VIP statistics, S-plot, and jack-knifed based confidence interval. S-plot combines the contribution/covariance (Cov(t,**X**)) and reliability/correlation (Corr(t,**X**)) from OPLS-DA model and helps to identify differential metabolites between classes [32]. Both of these two parameters have a theoretical minimum of −1 and maximum of 1. With a significance level of 0.05, a correlation coefficient (Corr(t,**X**)) of ±0.58 was adopted as a cutoff value to select the variables that are most correlated with the

OPLS-DA discriminant scores (predictive component). The correlation coefficients were calculated using Pearson linear correlation coefficients incorporated in MATLAB R2007a (The MathWorks, Inc., Natick, MA, USA. Details are available in the Supplementary Materials). The loading plot with $CIJF_{jk}$ displayed the uncertainty of each variable and the smaller span of confidence interval renders more creditability on the selected variable. In this study, those variables with $CIJF_{jk}$ across zero were excluded. Therefore, we merely chose those variables meeting the threefold criteria (i.e., VIP > 1, $|Corr(t,\mathbf{X})| > 0.58$, and the span of $CIJF_{jk}$ excluding zero) as the most significant and reliable variables, which could serve as candidate biomarkers for CUMS.

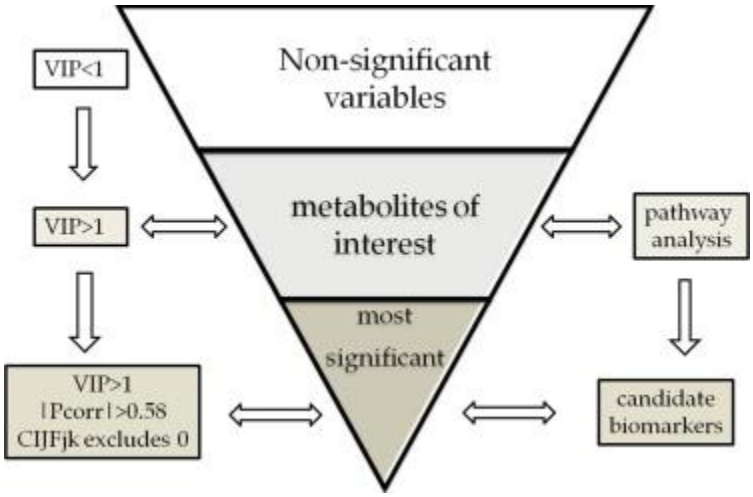

Fig. 2. General purpose and procedure of variable selection. VIP statistics (VIP > 1.0) was initially opted to select the significant variables for biological pathway analysis while multi-criteria assessment (MCA) was used for choosing the most significant and reliable variables (candidate biomarkers) by using a combination of VIP statistics, S-plot, and jack-knifed based confidence interval.

2.5. Qualitative and quantitative analyses [40]

Compound identification was processed by comparison of the ion fragments with those present directly in the GC/MS spectral databases including NIST, Wiley, and NBS, ultimately verified by reference compounds available. Additionally, the concentration of each verified metabolite was quantified via the corresponding calibration curve and was expressed as the relative percentage change. More details are provided in the Supporting Materials.

3. Results

3.1. Sucrose preference test and body weight gain

The CUMS-treated rats consumed significantly less sucrose solution as compared to the healthy controls (66 ± 8% versus 96 ± 4%, $P < 0.01$, unpaired *t*-test), indicating depressive-like behavioral state (e.g., impairment of hedonic reactivity) in the stressed rats. Meanwhile, the CUMS-treated rats suffered significantly slower body weight gain than the healthy ones (45.8 ± 8.7 g versus 78.2 ± 4.0 g, $P < 0.05$). Details are available in the Supplementary Materials. All these findings confirmed the stress-related effects on the rat.

3.2. GC/MS spectra of brain tissue samples

Typical GC/MS total ion current (TIC) chromatograms of each part of brain tissue samples from the CUMS-treated rats (Supporting Fig. 1a–d) and the healthy rats (Supporting Fig. 1e–h) are illustrated. Visual inspection of these spectra revealed obvious difference either among discrete brain regions or between the CUMS-treated group versus the healthy control for each brain region, but the complexity of GC/MS spectra hampered further comparison between classes. Thus, we used our custom GC/MS analytical protocol in conjunction with peak deconvolution procedure [29], and obtained a three-dimensional matrix consisting of 48 samples, 161 peak indices (RT-M/Z pairs) presumably representing individual metabolites throughout all the tissue samples, and 161 peak intensity. The resulting data set was subsequently analyzed to extract useful information by multivariate statistics including PCA and OPLS-DA.

3.3. Multivariate statistics

A five-component PCA model was initially obtained from the GC/MS data set deriving from all the tissue samples (Table 1, Supporting Fig. 2a and b). The inherent metabolic difference among brain regions and in relation to stress factors can be reflected by a 2D-PCA scores plot (PC1 versus PC3, Fig. 3). In this map, metabolic profiles of cerebral cortex and thalamus can be clearly separated from those of hippocampus and the remaining brain regions by the PC1 either in the CUMS-treated rats or in the healthy controls, while the stress-related metabolic variation was also readily noticed in the PC3. These findings mostly suggested that metabolic variations depicted by the PCA scores map were correlated with brain tissue regions and stress state as well. To gain more insights into stress-related metabolic variations in each brain compartment, the initial data set was divided into four subsets according to topographical region. The model quality was summarized in the Table 1.

Table 1.
Summary of the parameters for assessing modeling quality

	PCA model		**OPLS-DA model**			
	No[c]	R^2X_{cum}[a]	**No**[c]	R^2X_{cum}[a]	R^2Y_{cum}[a]	Q^2Y_{cum}[a]
Cerebral cortex	3	0.65	1P + 1O[b]	0.40	0.96	0.71
Hippocampus	3	0.76	1P + 1O	0.64	0.97	0.85
Thalamus	3	0.75	1P + 1O	0.45	0.98	0.78
Remaining regions	3	0.64	1P + 1O	0.45	0.91	0.60
All tissue samples	5	0.67				

[a] $R^2\mathbf{X}_{cum}$ and $R^2\mathbf{Y}_{cum}$ are the cumulative modeled variation in **X** and **Y** matrix, respectively, and $Q^2\mathbf{Y}_{cum}$ is the cumulative predicted variation in **Y** matrix. The values of these parameters close to 1.0 indicate a robust mathematical model with a reliable predictive accuracy.
[b] 1P + 1O, one predictive component and one orthogonal Component for establishing the OPLS-DA model.
[c] No, the number of components.

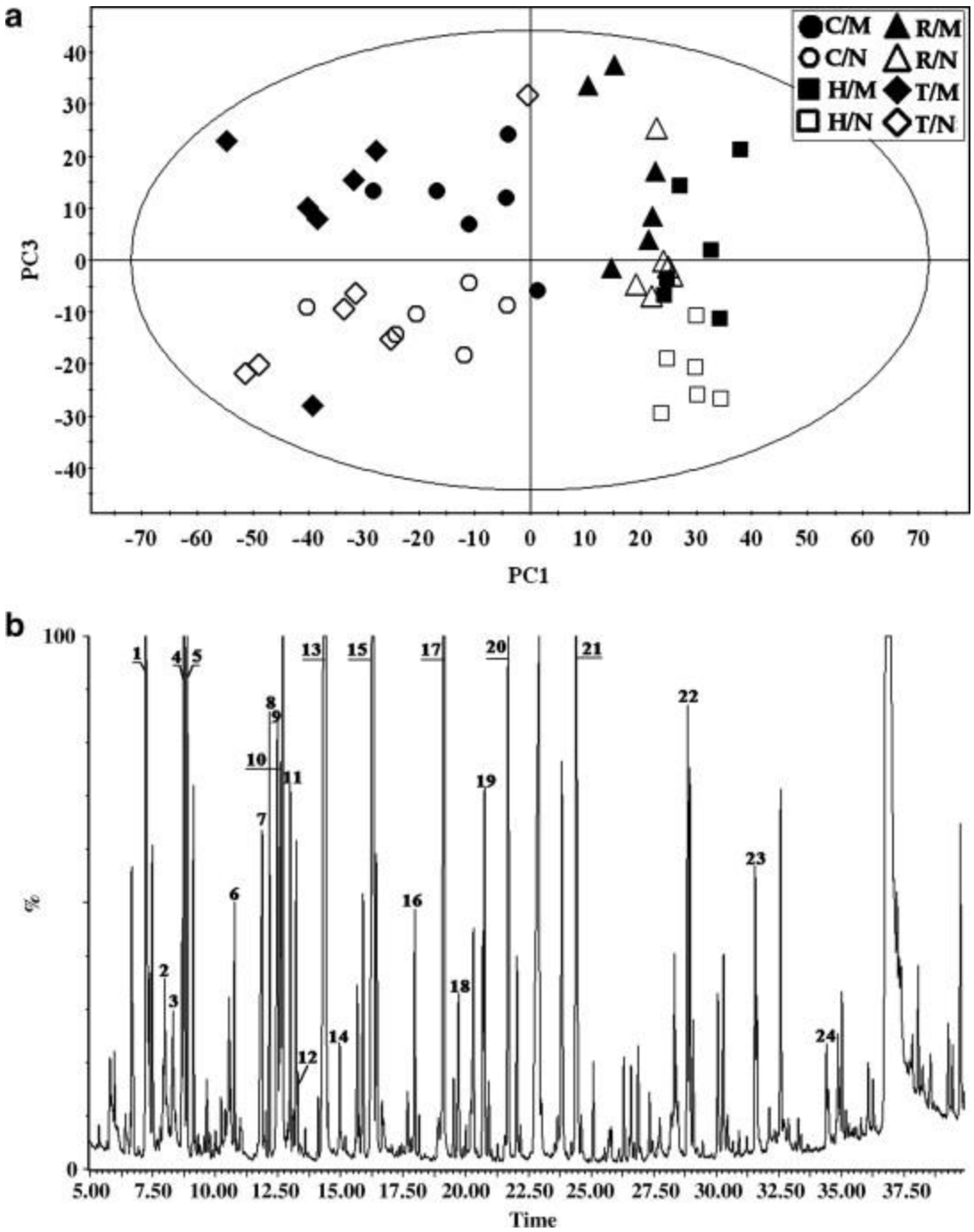

Fig. 3. (a) PCA scores map of GC/MS data derived from brain tissue samples in the CUMS-treated group and the healthy control. C, cerebral cortex; H, hippocampus; T, thalamus; R, the remaining brain regions; N, the healthy control group; and M, the CUMS-treated group. Each dot denotes an individual rat. (b) Typical GC/MS total ion current (TIC) chromatogram of cerebral cortex from a healthy rat. The keys are provided in the Table 2.

3.4. Cerebral cortex

A 3D-PCA scores map showed that obvious separation of metabolic profiles between the CUMS-treated group and the healthy control occurred in the PC1 (Fig. 4a). The inter-class

variation as indicated by the PCA map was also verified by the complete and significant separation ($P < 0.01$) in a cross-validated OPLS-DA score map (Fig. 4b). Additionally, the higher overlap between cross-validated scores (t[1]cv, i; i = 1–6) and the model scores (t[1]p) for most of cerebral cortex samples suggested the stability and reliability of the OPLS-DA model.

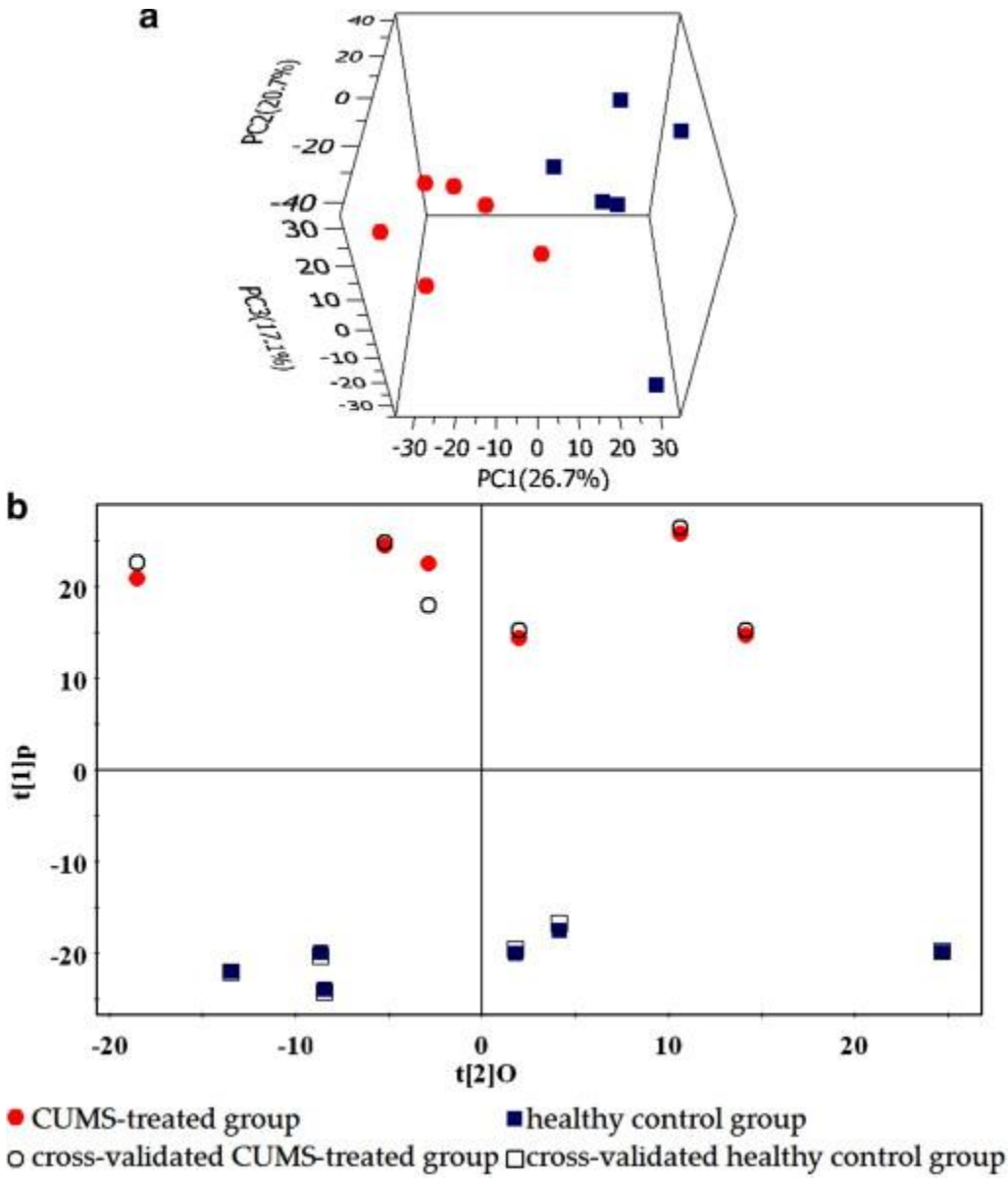

Fig. 4. (a) 3D-PCA scores map and (b) 1D cross-validated OPLS-DA score map of GC/MS data deriving from cerebral cortex samples obtained from the CUMS-treated group versus the healthy control group (n = 6 *per* group). The modeled score value (t[1]p), the 6th round cross-validated score value (t[1]cv$_6$), and orthogonal score value (t[2]o) for each individual are illustrated for each observation.

To identify which variables are accountable for such significant separation, VIP statistics was firstly used to pre-select variables (Fig. 5a). According to the criterion for VIP statistics (VIP > 1), a total of 28 variables were obtained for their most contribution in discriminating

metabolic profiles between the two classes. Subsequently, relying on the MCA strategy including VIP > 1, $|\mathrm{Corr}(t,\mathbf{X})| > 0.58$, and the span of CIJF_{jk} excluding zero, 17 variables presumably representing individual metabolites could be considered as candidate biomarkers (Fig. 5a–c, Table 2). For example, *N*-acetyl aspartate (NAA) was labeled with a red arrow in the VIP plot, S-plot, and loading plot with CIJF_{jk}. NAA has the top VIP value of 5.4, which means that NAA contributed most for class discrimination. In the S-plot, NAA displayed the highest positive correlation coefficient ($\mathrm{Corr}(t,\mathbf{X}) = 0.77$) and was therefore reliable for class separation. Similar information was shown by CIJF_{jk} plot where NAA had a smaller span of confidence interval. Thus, NAA was surely selected for further investigation of biological significance.

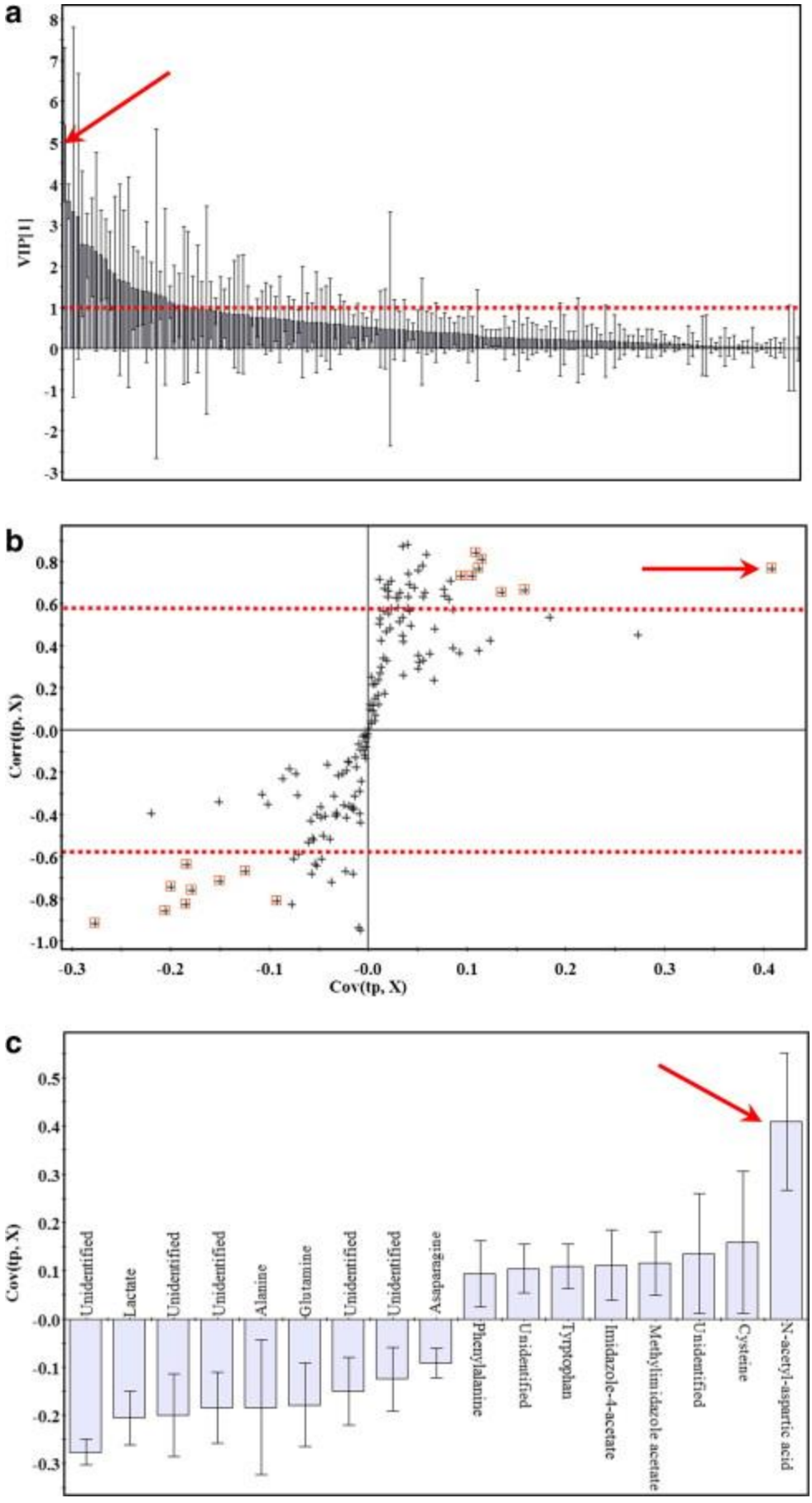
a
VIP[1]
b
Corr(tp, X)
Cov(tp, X)
c
Cov(tp, X)
Unidentified
Lactate
Unidentified
Unidentified
Alanine
Glutamine
Unidentified
Unidentified
Asaparagine
Phenylalanine
Unidentified
Tryptophan
Imidazole-4-acetate
Methylimidazole acetate
Unidentified
Cysteine
N-acetyl-aspartic acid

Fig. 5. VIP plot (a), S-plot (b), and loading plot with $CIJF_{jk}$ (c) from OPLS-DA modeling of GC/MS spectral data deriving from all the cerebral cortex samples.

Table 2.
A list of significant compounds accountable for class discrimination

Key	**Compound**	**C**	**H**	**T**	**R**	**Metabolic function**
1	Lactate	↓* Δ	–	↓* Δ	–	Glucose metabolism
2	Imidazole-4-acetate	↑* Δ	↓	–	↓	Histamine metabolism
3	Methylimidazole acetate	↑* Δ	↑	–	↓*	Histamine metabolism
4	Alanine[a]	↓* Δ	↑*	↓*	↑	Aspartate metabolism
5	Glycine[a]	↑	↑*	↑* Δ	↑ Δ	Inhibitory neurotransmitter
6	Valine[a]	–	↑* Δ	↑* Δ	↑* Δ	Glutamate synthesis
7	Serine	↓	↓ Δ	↑* Δ	↑	Glycine metabolism
8	Leucine[a]	–	↑* Δ	↑	↑* Δ	Glutamate synthesis
9	Iso-leucine[a]	–	–	–	↑	Glutamate synthesis
10	Threonine[a]	↑	–	↑* Δ	↑	Glycine metabolism
11	Proline[a]	–	↑* Δ	–	↑* Δ	Proline metabolism
12	Asparagine[a]	↓* Δ	–	–	–	Aspartate metabolism
13	*N*-Acetyl aspartate	↑* Δ	↑* Δ	↓* Δ	↓* Δ	Aspartate metabolism
14	3-Indolepropionate	–	↓* Δ	–	–	Amino acid metabolism
15	Aspartate[a]	↓	↑	↓	–	Excitatory neurotransmitter
16	Methionine[a]	–	–	–	↑* Δ	Cysteine metabolism
17	Glutamate[a]	–	↑* Δ	↓	↓*	Excitatory neurotransmitter
18	Glutamine	↓* Δ	↓ Δ	–	–	Glutamate metabolism
19	Phenylalanine[a]	↑* Δ	↑* Δ	↑* Δ	↑* Δ	Tyrosine metabolism
20	Cysteine	↑* Δ	–	–	↓	Cysteine metabolism
21	Hexadecanoic acid	–	–	↑	↓ Δ	Fatty acid biosynthesis
22	Lysine[a]	–	↓* Δ	↑ Δ	↑	Amino acid metabolism

Key	Compound	C	H	T	R	Metabolic function
23	Arachidonic acid	–	–	↑* △	–	Lipid metabolism
24	Tryptophan[a]	↑* △	–	↑* △	–	Serotonin metabolism

The star (*) represents the |Corr(t,**X**)| > 0.58 and the triangle (△) means the span of $CIJF_{jk}$ excluding zero. The short dash line (–) indicates no significant variation. The raw data are provided in the Supplementary Materials. Abbreviations: C, cerebral cortex; H, hippocampus; T, thalamus; and R, the remaining brain regions.

[a] These metabolites are verified by reference compounds available. The arrow denotes the VIP value greater than 1.0 and the up- (or down-) regulation of the arrow represents the relative increased (or decreased) concentration in the CUMS-treated group as compared to the healthy control.

3.5. Hippocampus, thalamus, and the remaining brain tissues

GC/MS spectral datasets deriving from other three discrete brain regions were processed in a similar manner. Each 3D-PCA scores map

GC/MS spectral datasets deriving from other three discrete brain regions were processed in a similar manner. Each 3D-PCA scores map showed clear separation tendency of metabolic profiles between the CUMS-treated group and the healthy control (Supporting Fig. 3a–c). Three additional OPLS-DA models confirmed the class separation for each brain region according to the pathophysiological status and the cross-validated OPLS-DA scores map indicated the stability and reliability of each OPLS-DA model (Supporting Fig. 3d–f).

3.6. Summary of significant metabolites from four discrete brain tissues

Based on MCA for OPLS-DA of four discrete brain regions, a total of 43 significant variables were finally obtained. Among those significant variables, 24 metabolites were readily identified by comparing the ion fragments with those from our GC/MS spectral databases (Table 2), and 14 amino acids were verified using reference compounds available. Furthermore, in order to verify the CUMS-related metabolic variation in discrete brain regions, quantitative analysis was carried out on these 14 amino acids. The accurate percentage of these metabolites was calculated (Table 3).

Table 3.
Relative percentage of variation for 14 amino acids using quantitative analysis

Key	Compound	C	H	T	R
4	Alanine	↓23% *	↓18%[a]	–	–
5	Glycine	–	–	↑13%	↑24%
6	Valine	–	–	↑18%	↑70% *
8	Leucine	↓18%	↑13% *	↑13%	↑57% *

Key	Compound	C	H	T	R
9	Iso-leucine	–	–	↑29% *	↑67% *
10	Threonine	↓14%[a]	–	↑38%	↑22% *
11	Proline	↓13%	–	–	↑19%
12	Asaparagine	↓44% *	–	–	↑34%
15	Aspartate	↓13% *	–	–	–
16	Methionine	–	↑18%	–	↑23%
17	Glutamate	–	–	–	↑16%[a]
19	Phenylalanine	–	–	↑20%	↑37% *
22	Lysine	↓22%	↓24%	↑23%	↑37%
24	Tyrptophan	–	↓15%	↑33% *	–

[a] Inconsistency with multivariate statistics.

* Statistical significance ($P < 0.05$, unpaired student's *t*-test).

4. Discussion

With the aim of monitoring the local metabolic changes in complex neural disorder–chronic unpredictable mild stress, we used a GC/MS technique to profile the metabolites present in four discrete brain regions, including cerebral cortex, hippocampus, thalamus, and the remaining regions in the rats exposed repeatedly to nine different stressors for four weeks in a random order. Cerebral cortex is the largest part of the brain related with sophisticated brain functions such as thought and action; thalamus and hippocampus are important parts in the limbic system, which is associated with emotional reactions and has been an interest in clinical depression research. Thus, we focused on those four distinct brain regions for their specific biological functions. To our great interest, not all the metabolic variations occur consistently in the four brain regions in this study. For instance, lactate, as one major end product of both aerobic and anaerobic glycolysis [41], was found significantly decreased only in cerebral cortex and thalamus with sensory and motor functions. Such abnormal alteration might indicate that energy metabolism in cortex and thalamus was an outcome of long-time fatigue of CUMS-treated rats in our study. In terms of biological functions in other brain regions, a more systematic study involving molecular biology is needed to investigate the biochemical variations of each brain region in the future work.

4.1. Identification of significant metabolites

Relying on the four subsets of significant metabolites, many metabolites significantly altered between the CUMS-treated group and the healthy control in a certain brain region but did not feature across all the brain regions whereas some differential metabolites did not display consistent changing trend across different brain regions. Despite of such inconsistence, the

disturbed metabolic pathways, particularly disorder of amino acid metabolism, could be prominently reflected in the brain [42] (Fig. 6).

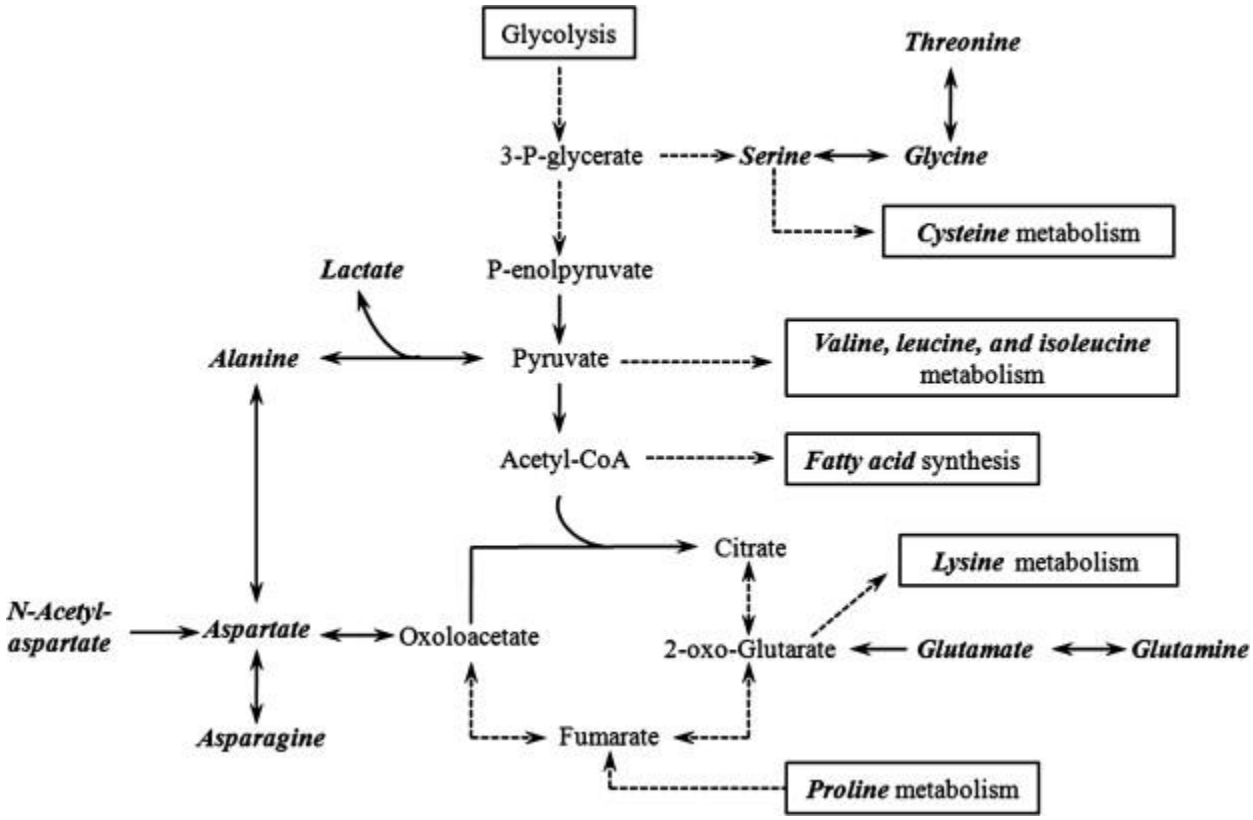

Fig. 6. The perturbed metabolic pathways especially amino acid metabolism in the stress-rats. Compound detected in this study was shown in bond italic font.

4.2. Quantitative analysis

According to the MCA measure, a number of 14 amino acids was identified and quantified, which is considered as the most significant and reliable metabolites closely associated with CUMS. Quantitative analysis not only provides accurately subtle metabolic variation in the brain tissues but also can assess the findings from multivariate statistics. Taking into consideration that various factors, e.g., systemic errors in weighing, extraction, and derivatization of tissue samples possibly interfered with the stress-related metabolic variation, we set a minimum percentage (13%) with statistical significance ($P < 0.05$) as a critical threshold (Table 3). It is reasonable that the concentration changes for the majority of these amino acids are fairly consistent with the results from multivariate statistics, except for inconsistent alteration of three compounds (threonine in cerebral cortex; alanine in hippocampus; glutamate in the remaining regions). Such inconsistency is partially due to the fact that signals of impurities and confounding noise might distort the data set during normalization and scaling procedures necessary for multivariate statistics [43] and [44]. Therefore, the present work suggested that: (1) MCA for multivariate statistics could be an efficient and robust approach for the selection of candidate biomarker metabolites; (2) quantitative analysis of significant metabolites should be accompanied to verify the accuracy of multivariate statistics.

4.3. Amino acid metabolism

The most significant alterations attributed to the disorder of amino acid metabolism. These differential amino acids can be categorized into two classes: excitatory/inhibitory neurotransmitters and branched-chain amino acids (BCAAs). While the intensity of glycine was significantly increased across the four brain regions, the variation of aspartate in each brain region appeared to be inconsistent towards the stressors. Interestingly, the ratio of glycine to aspartate (an important inhibitory/excitatory pair) was increased across all the brain regions especially, significantly in cortex, thalamus and the remaining brain regions ($P < 0.05$), which may suggest the importance of the intricate balance between inhibitory and excitatory amino acids to maintain normal brain function [24] and [45]. In addition, serving as an important excitatory neurotransmitter in the mammalian CNS, glutamate was decreased in thalamus and the remaining brain regions but increased in hippocampus. This finding suggested that glutamate could participate actively in the synthesis of glucose and ketone bodies for the brain in response to xenobiotic stimuli while the excessive release of glutamate could be associated with the brain impairment [46]. In parallel, the significant reduction of glutamine that can release amine and produce glutamate to maintain nitrogen balance was observed in cerebral cortex and hippocampus. Taken together, these results may be indicative of stress-induced deficiency in glutamate–glutamine neurotransmitter cycling.

In this study, BCAAs including leucine, isoleucine, and valine, were increased in each brain region of the CUMS-induced rats as compared to that of the healthy controls. These BCAAs can transport quickly across the blood-brain barrier as major amino group donors for the synthesis of brain glutamate. Recent studies have demonstrated that BCAAs, especially leucine, contribute most to the derivation in astrocytes of glutamate and glutamine so as to maintain the homeostasis of brain nitrogen [47]. Additionally, the increased concentration of tryptophan was observed in cerebral cortex and thalamus from the stressed rat brain. The neurotransmitter 5-hydroxy-tryptamine (5-HT) is sensitive to the fraction of tryptophan available in plasma for transport into the brain, as well as the concentration of BCAAs that are transported via the same carrier system. Thus, the increased concentration of both tryptophan and BCAAs could indicate the disturbed release of brain 5-HT that is highly related with the central fatigue [48]. Hence, the increased BCAAs and tryptophan may suggest the impaired glutamate homeostasis in the brain as well as reflect central fatigue in response to the chronic stress.

4.4. NAA metabolism

The significant perturbation of NAA was also responsible for discriminating metabolic profiles between the CUMS-treated rats and the healthy controls, showing an increase in cerebral cortex and hippocampus while a decrease in thalamus and the remaining brain regions. NAA is synthesized in the mitochondria and considered as a marker for neuronal density [24] and [49]. Generally, decrease in the concentration of NAA occurs in conditions of neuronal damage or loss, such as chronic psychosocial stress and perinatal stress [50] and [51]. Meanwhile, the increase of NAA in two brain regions may reflect the stress-induced complementary increase of amino acids for its metabolic function of transferring amino nitrogen from the mitochondrion to the cytoplasm [52]. It is clear that each subtle yet significant variation of metabolites has its own biochemical function in response to or resulting in chronic mild stress (Table 3).

In summary, the combined use of GC/MS analytical technique and multivariate statistics facilitate the discrimination of metabolic profiles in different brain tissues including cortex, hippocampus, thalamus, and the remaining brain regions between the CUMS-treated rats and the healthy controls. The disorder of amino acid metabolism is significant across all the brain tissues, partially suggesting the impairment of neural activity of CNS. In addition, the utility of MCA in variable selection greatly improves reliability of the differential metabolites. Using this tissue-targeted metabolic profiling strategy, we are able to recognize an integrated, perturbed biological pathway-disorders of amino acid metabolism associated closely with the stress-related pathological variation in the brain.

Acknowledgements

We are grateful to Mingmei Zhou (Shanghai University of Traditional Chinese Medicine), and Houkai Li (Shanghai Jiao Tong University) for the dissection of discrete brain regions in animal experiment. This work is finically supported by the National Basic Research Program, Grant Nos. 2007CB914700 and 2007CB511900.

References

[1] Narrow, W.E. (1998) One-year prevalence of mental disorders, excluding substance use disorders, in the US: NIMH ECA prospective data. One-year Prevalence of Depressive Disorders Among Adults 18 and Over in the US: NIMH ECA Prospective Data. Population Estimates Based on US Census Estimated Residential Population Age 18 and Over on July 1, 1998.
[2] http://www.nimh.nih.gov/health/publications/depression/complete-publication.shtml.
[3] M. Papp, P. Willner and R. Muscat, An animal model of anhedonia: attenuation of sucrose consumption and place preference conditioning by chronic unpredictable mild stress, *Psychopharmacology* **104** (1991), pp. 255–259.
[4] P. Willner, A. Towell, D. Sampson, S. Sophokleous and R. Muscat, Reduction of sucrose preference by chronic unpredictable mild stress, and its restoration by a tricyclic antidepressant, *Psychopharmacology* **93** (1987), pp. 358–364.
[5] S. Bhatnagar, C. Vining, V. Iyer and V. Kinni, Changes in hypothalamic-pituitary-adrenal function, body temperature, body weight and food intake with repeated social stress exposure in rats, *J. Neuroendocrinol.* **18** (2006), pp. 13–24.
[6] A.J. Grippo, J.A. Moffitt and A.K. Johnson, Cardiovascular alterations and autonomic imbalance in an experimental model of depression, *Am. J. Physiol. Regul. Integr. Comp. Physiol.* **282** (2002), pp. R1333–R1341.
[7] L.R. Lucas, Z. Celen, K.L. Tamashiro, R.J. Blanchard, D.C. Blanchard, C. Markham, R.R. Sakai and B.S. McEwen, Repeated exposure to social stress has long-term effects on indirect markers of dopaminergic activity in brain regions associated with motivated behavior, *Neuroscience* **124** (2004), pp. 449–457.
[8] M. Martinez, P.J. Phillips and J. Herbert, Adaptation in patterns of c-fos expression in the brain associated with exposure to either single or repeated social stress in male rats, *Eur. J. Neurosci.* **10** (1998), pp. 20–33.
[9] V. Sergeyev *et al.*, Neuropeptide expression in rats exposed to chronic mild stresses, *Psychopharmacology* **178** (2005), pp. 115–124.
[10] P. Willner, Validity, reliability and utility of the chronic mild stress model of depression: a 10-year review and evaluation, *Psychopharmacology* **134** (1997), pp. 319–329.

[11] J.K. Nicholson, J.C. Lindon and E. Holmes, 'Metabonomics': understanding the metabolic responses of living systems to pathophysiological stimuli via multivariate statistical analysis of biological NMR spectroscopic data, *Xenobiotica* **29** (1999), pp. 1181–1189.
[12] O. Fiehn, Metabolomics – the link between genotypes and phenotypes, *Plant Mol. Biol.* **48** (2002), pp. 155–171.
[13] A. Malmendal, J. Overgaard, J.G. Bundy, J.G. Sorensen, N.C. Nielsen, V. Loeschcke and M. Holmstrup, Metabolomic profiling of heat stress: hardening and recovery of homeostasis in Drosophila, *Am. J. Physiol. Regul. Integr. Comp. Physiol.* **291** (2006), pp. R205–R212.
[14] J. Overgaard, A. Malmendal, J.G. Sorensen, J.G. Bundy, V. Loeschcke, N.C. Nielsen and M. Holmstrup, Metabolomic profiling of rapid cold hardening and cold shock in Drosophila melanogaster, *J. Insect Physiol.* **53** (2007), pp. 1218–1232.
[15] C.R. Teague *et al.*, Metabonomic studies on the physiological effects of acute and chronic psychological stress in Sprague-Dawley rats, *J. Proteome Res.* **6** (2007), pp. 2080–2093.
[16] X. Wang *et al.*, Metabolic regulatory network alterations in response to acute cold stress and ginsenoside intervention, *J. Proteome Res.* **6** (2007), pp. 3449–3455.
[17] Y. Wang *et al.*, Experimental metabonomic model of dietary variation and stress interactions, *J. Proteome Res.* **5** (2006), pp. 1535–1542.
[18] J.T. Brindle *et al.*, Rapid and noninvasive diagnosis of the presence and severity of coronary heart disease using 1H-NMR-based metabonomics, *Nat. Med.* **8** (2002), pp. 1439–1444.
[19] D.B. Kell, Systems biology, metabolic modelling and metabolomics in drug discovery and development, *Drug Discov. Today* **11** (2006), pp. 1085–1092.
[20] J.C. Lindon, E. Holmes and J.K. Nicholson, Metabonomics in pharmaceutical R&D, *FEBS J.* **274** (2007), pp. 1140–1151.
[21] J.K. Nicholson, J. Connelly, J.C. Lindon and E. Holmes, Metabonomics: a platform for studying drug toxicity and gene function, *Nat. Rev. Drug Discov.* **1** (2002), pp. 153–161.
[22] O. Beckonert, H.C. Keun, T.M. Ebbels, J. Bundy, E. Holmes, J.C. Lindon and J.K. Nicholson, Metabolic profiling, metabolomic and metabonomic procedures for NMR spectroscopy of urine, plasma, serum and tissue extracts, *Nat. Protoc.* **2** (2007), pp. 2692–2703.
[23] C.Y. Lin, H. Wu, R.S. Tjeerdema and M.R. Viant, Evaluation of metabolite extraction strategies from tissue samples using NMR metabolomics, *Metabolomics* **3** (2007), pp. 55–67.
[24] M.R. Pears, J.D. Cooper, H.M. Mitchison, R.J. Mortishire-Smith, D.A. Pearce and J.L. Griffin, High resolution 1H NMR-based metabolomics indicates a neurotransmitter cycling deficit in cerebral tissue from a mouse model of Batten disease, *J. Biol. Chem.* **280** (2005), pp. 42508–42514.
[25] H. Wu, A.D. Southam, A. Hines and M.R. Viant, High-throughput tissue extraction protocol for NMR- and MS-based metabolomics, *Anal. Biochem.* **372** (2008), pp. 204–212.
[26] J. Trygg, E. Holmes and T. Lundstedt, Chemometrics in metabonomics, *J. Proteome Res.* **6** (2007), pp. 469–479.
[27] E.M. Lenz and I.D. Wilson, Analytical strategies in metabonomics, *J. Proteome Res.* **6** (2007), pp. 443–458. [28] N. Kettaneh, A. Berglund and S. Wold, PCA and PLS with very large data sets, *Comput. Stat. Data Anal.* **48** (2005), pp. 69–85.
[29] Y. Ni, M. Su, Y. Qiu, M. Chen, Y. Liu, A. Zhao and W. Jia, Metabolic profiling using combined GC–MS and LC–MS provides a systems understanding of aristolochic acid-induced nephrotoxicity in rat, *FEBS Lett.* **581** (2007), pp. 707–711.
[30] S. Wold, M. Sjostrom and L. Eriksson, PLS-regression: a basic tool of chemometrics, *Chemom. Intell. Lab. Syst.* **58** (2001), pp. 109–130.

[31] M. Hedenstrom, S. Wiklund, B. Sundberg and U. Edlund, Visualization and interpretation of OPLS models based on 2D NMR data, *Chemom. Intell. Lab. Syst.* **92** (2008), pp. 110–117.
[32] S. Wiklund *et al.*, Visualization of GC/TOF-MS-based metabolomics data for identification of biochemically interesting compounds using OPLS class models, *Anal. Chem.* **80** (2008), pp. 115–122.
[33] Y. Qiu, M. Su, Y. Liu, M. Chen, J. Gu, J. Zhang and W. Jia, Application of ethyl chloroformate derivatization for gas chromatography–mass spectrometry based metabonomic profiling, *Anal. Chim. Acta* **583** (2007), pp. 277–283.
[34] M. Bylesjo, M. Rantalainen, O. Cloarec, J.K. Nicholson, E. Holmes and J. Trygg, OPLS discriminant analysis: combining the strengths of PLS-DA and SIMCA classification, *J. Chemom.* **20** (2006), pp. 341–351. [35] S. Wold, K. Esbensen and P. Geladi, Principal component analysis, *Chemom. Intell. Lab. Syst.* **2** (1987), pp. 37–52.
[36] R.A. van den Berg, H.C. Hoefsloot, J.A. Westerhuis, A.K. Smilde and M.J. van der Werf, Centering, scaling, and transformations: improving the biological information content of metabolomics data, *BMC Genomics* **7** (2006), p. 142.
[37] J. Trygg and S. Wold, Orthogonal projections to latent structures (O-PLS), *J. Chemom.* **16** (2002), pp. 119–128.
[38] J.A. Westerhuis, H.C.J. Hoefsloot, S. Smit, D.J. Vis, A.K. Smilde, E.J.J. van Velzen, J.P.M. van Duijnhoven and F.A. van Dorsten, Assessment of PLSDA cross validation, *Metabolomics* **4** (2008), pp. 81–89. [39] J.C. Lindon *et al.*, Summary recommendations for standardization and reporting of metabolic analyses, *Nat. Biotechnol.* **23** (2005), pp. 833–838.
[40] Lin, J.C. et al. (in press). Multiparametric analysis of amino acids and organic acids in rat brain tissues using GC/MS. J. Sep. Sci.
[41] A. Schurr, Lactate: the ultimate cerebral oxidative energy substrate?, *J. Cereb. Blood Flow Metab.* **26** (2006), pp. 142–152.
[42] http://www.genome.jp/kegg/.
[43] R. Goodacre *et al.*, Proposed minimum reporting standards for data analysis in metabolomics, *Metabolomics* **3** (2007), pp. 231–241.
[44] D.I. Broadhurst and D.B. Kell, Statistical strategies for avoiding false discoveries in metabolomics and related experiments, *Metabolomics* **2** (2006), pp. 171–196.
[45] H.S. Sharma, Interaction between amino acid neurotransmitters and opioid receptors in hyperthermia-induced brain pathology, *Prog. Brain Res.* (2007), pp. 295–317.
[46] M.W. Warenycia, S.B. Kombian and R.J. Reiffenstein, Stress-induced increases in brainstem amino acid levels are prevented by chronic sodium hydrosulfide treatment, *Neurotoxicology* **11** (1990), pp. 93–97.
[47] Y. Shimomura and R.A. Harris, Metabolism and physiological function of branched-chain amino acids: discussion of session 1, *J. Nutr.* **136** (2006), pp. 232S–233S.
[48] E. Blomstrand, A role for branched-chain amino acids in reducing central fatigue, *J. Nutr.* **136** (2006), pp. 544S–547S.
[49] K.K. Bhakoo, T. Craig and D. Pearce, *N*-acetyl aspartate metabolism in neural cells, *Adv. Exp. Med. Biol.* **576** (2006), pp. 27–47.
[50] R.E. Poland, C. Cloak, P.J. Lutchmansingh, J.T. McCracken, L. Chang and T. Ernst, Brain *N*-acetyl aspartate concentrations measured by H MRS are reduced in adult male rats subjected to perinatal stress: preliminary observations and hypothetical implications for neurodevelopmental disorders, *J. Psychiatr. Res.* **33** (1999), pp. 41–51.

[51] B. Czeh, T. Michaelis, T. Watanabe, J. Frahm, G. de Biurrun, M. van Kampen, A. Bartolomucci and E. Fuchs, Stress-induced changes in cerebral metabolites, hippocampal volume, and cell proliferation are prevented by antidepressant treatment with tianeptine, *Proc. Natl. Acad. Sci. USA* **98** (2001), pp. 12796–12801.
[52] S.L. Miller, Y. Daikhin and M. Yudkoff, Metabolism of *N*-acetyl-l-aspartate in rat brain, *Neurochem. Res.* **21** (1996), pp. 615–618.

SUPPLEMENTARY MATERIALS

Metabolic profiling reveals disorder of amino acid metabolism in four brain regions from a rat model of chronic unpredictable mild stress

Yan Ni [a, †], Mingming Su [a, †], Jinchao Lin [a], Xiaoyan Wang [b], Yunping Qiu [b], Aihua Zhao [a], Tianlu Chen [b], Wei Jia [a, c, *]

[a]School of Pharmacy and [b]Shanghai Institute for Systems Biomedicine, Shanghai Jiao Tong University, Shanghai, 200240, P.R.China, [c]Shanghai University of Traditional Chinese Medicine, Shanghai, P.R. China

S1. SUPPORTING METHODS AND RESULTS

This section involves animal handling and sampling , sucrose preference test, open-filed test, sample preparation, GC/MS assay, data acquisition and pretreatment, and quantitative analysis.

S1-1 Animal handling and sampling

The study was approved by national legislations of China and local guidelines. A total of twelve eight-week-old male Sprague-Dawley (S.D.) rats (weighing 200 ± 20 g) was

[*] Corresponding author. Fax: (86)-021-6293-2292.Email address: weijia@sjtu.edu.cn
[†] Contributed equally to this work.

Abbreviations: NMR, nuclear magnetic resonance; MS, mass spectrometry; GC/MS, gas chromatography/ mass spectrometry; PCA, principal component analysis; OPLS-DA, orthogonal partial least squares project to latent structures- discriminant analysis; MCA, multi-criteria assessment; VIP, variable importance in the projection; CUMS, chronic unpredictable mild stress; SNS, sympathetic nervous system; CNS, central nervous systems; HPA, hypothalamic-pituitary-adrenocortical; ECF, ethyl chloroformate; $CIJF_{jk}$, jack-knifed confidence interval; NAA, N-acetyl aspartate; BCAAs, branched-chain amino acids.

commercially obtained from Shanghai Laboratory Animal Co. Ltd. (SLAC, Shanghai, China), and kept at a barrier system with regulated environment (24 ± 1 °C, 45 ± 15 % relative humidity, and 12h/12h light/dark cycle). The rats were fed with a certified standard rat chow and tap water *ad libitum*. After two-week acclimation, all of the rats were randomly divided into two groups (n = 6 *per* group): the healthy control group *versus* the CUMS-treated group in which the rats were repeatedly exposed to a set of chronic unpredictable mild stressors. The CUMS procedures includes nine different kinds of stressors as follows: 5 min of forced swimming in 15 °C water; exposure to an experimental room at 40 °C and -10 °C for 5 min, respectively; 24 hour of food deprivation and 24 hour of water deprivation, respectively; 6 unpredictable shocks: 15 V, 20 sec duration, one shock/10 sec; tail clamp for 1 min; inversion of light/dark cycle; 2 hour of restricted movement (confinement in a mouse cage). One stressor was applied *per* day and the whole stress procedure lasted for four weeks with a completely random order. The healthy control rats were housed undisturbed in another experiment room under the same condition. They had free access to tap water and food except for the period of water and food deprivation prior to the sucrose preference test. At the 4^{th} week of the entire experiment, all of the rats were sacrificed with sodium pentobarbital anesthesia (40 mg/100 g body weight, i.p.). Brain tissues including cerebral cortex, hippocampus, thalamus, and remaining brain regions were obtained from each rat carefully and instantly stored at -80 °C before assay.

S1-2 Sucrose preference test

The depressive-like behavioral state was assessed by a sucrose preference test as described. After a 20-hour period of water and food deprivation, each rat was subjected to

an individual metabolic cage in which two bottles containing water and 1% sucrose solution were placed. The ratio of the amount of sucrose solution to that of total solution ingested within one hour represented the parameter of hedonic behavior. Sucrose preference test was trained for three times before the commencement of the stress procedure.

S1-3 Open-field test

Open-field test was conducted in a quiet room between 13:00 and 15:00 p.m. at a rectangular arena 80×80 cm with 40-cm-high side walls, the floor marked with a grid dividing it into 25 equal-size squares. Each animal was placed in the central square at first and observed for 5 min. Scores were calculated by the amount of time that rats spent grooming and rearing (defined as standing upright on its hind legs, one score for once) and by the number of grid lines rats can cross using at least three paws (every grid crossed counts one score). In this study, reduced activity and curiosity of CUMS-induced rats was indicated by low horizontal and vertical scores (40±13 for CUMS-treated rats *versus* 72±24 for the healthy controls, $p < 0.05$), the depressive state was in accordance with the clinical psychomotor hysteresis symptoms of depression very well.

S1-4 Sample preparation

The extraction and two-step derivatization procedures were conducted as our previously described with minor modification. In brief, each 80-mg aliquot of brain tissue samples was homogenized (T10 basic ULTRA-TURRAX homogenizer, IKA® Group, Staufen, Germany) with 400 μL of ultrapure water (Milli-Q system, Millipore, USA) for 1 min in an ice bath, with the pH of the system being adjusted to 10.0 using about 10~20 μL of 7 mol/L NaOH. The resultant mixtures were centrifuged at 8, 000 *g* for 10 min at

4 °C to remove precipitates and debris. After a 400-μL aliquot of the supernatant was transferred to a screw-top glass tube, additional 200 μL of water, 400 μL of anhydrous ethanol, 100 μL of L-2-chlorophenylalanine (internal standard, Shanghai Intechem Tech. Co. Ltd., China), 100 μL of pyridine, and 50 μL of ethyl chloroformate (ECF, China National Pharmaceutical Group Corporation, Shanghai, China) were supplied for derivatization. The resultant ECF-derivatives was isolated and dried with anhydrous sodium sulfate for following GC/MS analysis.

Note: The purpose of the selected following paragraph from our accepted paper is to explain why we used a GC/MS method with ECF derivatization for studying neurochemical changes in the stress-related rat brain. (With the permission of all the coauthors in that paper)

The brain is a highly complex system embracing a vast array of mutually interacting endogenous, small-molecule metabolites with varied chemical properties and specific biological significance. These metabolites in brain tissue, typically, amino acids and fatty acids are intermediates in cellular metabolism and play an indispensable role in regulating neural activity of central nervous system. The variation of them are of high significance for understanding the underlying mechanisms of various neurological diseases. Therefore, great effort has been made to qualify and quantify these crucial compounds in the brain tissues.

GC-MS technique serves as a versatile analytical tool and allows simultaneous detection of different classes of metabolites in a single analysis. Such a technique exhibits satisfactory sensitivity and selectivity than conventional NMR approach, and a good reliability in structure identification of candidate biomarkers than LC-MS. Moreover,

ethyl chloroformate (ECF) derivatization, as a simple and robust procedure, has proven preferable in the determination of amino acids. This derivatization has been of considerable interest, as ECF is an inexpensive agent and the reaction can be performed directly in aqueous medium without requirement for sample heating, which greatly facilitates batch preparation and improves reproducibility in quantifying amino acids.

S1-5 GC/MS spectral acquisition

Each 1-μL of the analyte was injected into a HP-5ms capillary column (30 m × 250 μm i.d., 0.25-μm film thickness; 5%-phenyl-methylpolysiloxane bonded and crosslinked; Agilent J&W Scientific, Folsom, CA, USA) and analyzed by a hyphenated analytical technique, an Agilent 6890N gas chromatography coupled with an Agilent 5975B inert MSD mass spectrometry (Agilent Tech., CA, USA).

S1-6 Data pretreatment

All of the raw GC/MS spectral data files were converted to NetCDF format via data analysis interface of the Agilent Instrument (Agilent Tech., CA, USA). Each data file was extracted using our custom scripts in the MATLAB R2007a (The MathWorks, Inc., Natick, MA, USA), where data pretreatment procedures such as baseline correction, peak deconvolution and alignment, exclusion of internal standard and solvent peaks, and normalization to the total chromatogram were constructed afterwards. The output data were organized in a three-dimensional matrix encompassing arbitrarily annotated peak indices (*RT-M/Z* pairs), sample names (observations), and all of the peak areas (variables).

S1-7 Correlation coefficients

Correlation coefficients were calculated by using Pearson linear correlation

coefficients incorporated in MATLAB R2007a (The MathWorks, Inc., Natick, MA, USA). Firstly, all the GC/MS data were set as X matrix, and OPLS-DA discriminant scores in the first predictive component as Y matrix. Then, we repeatedly calculated the correlation coefficients of each variable and discriminant scores using Matlab function [R, p]=corrcoef (X, Y). [R,P]=corrcoef(...) also returns P, a matrix of p-values for testing the hypothesis of no correlation. Each p-value is the probability of getting a correlation as large as the observed value by random chance, when the true correlation is zero. If P(i,j) is small, say less than 0.05, then the correlation R(i,j) is significant.

S1-8 Analytical assay and quantitative analysis

In this study, we firstly established a reliable and efficient method for global analysis of water extracts from brain tissue samples. This method has been detailedly described elsewhere (*unpublished paper*). Briefly, the protocol was extensively evaluated using brain tissue samples and a set of 23 reference standards encompassing amino acids, amines, and organic acids. Acceptable calibration curves were obtained over a wide concentration range, 0.2-35.0 μg/mL for standards and 0.067-0.417 mg/μL (w/v, tissue/water) for brain tissue samples. The precision of the samples analyzed was mostly lower than 10% for both the mixed standard solution and the brain tissue samples. The brain tissue samples exhibited good stability within 48 hours with RSD generally less than 15%.

Quantitative analysis of the 14 amino acids was herein carried out using the analytical curves that were constructed using solutions at a concentration of 0.2, 0.5, 1.0, 5.0, 10.0, 15.0, 20.0, 25.0, or 35.0 μg/ml. The selected ion that exhibits the strongest response without disturbance was used to calculate the content for each amino acid in each brain

region. The expression can be described as

$$X_{sample,\,i} = X_{standard,\,i} \times (Y_{sample,\,i} / Y_{standard,\,i} - B_{adj,\,i}) / K_{adj,\,i}$$

$X_{sample,\,i}$: Concentration of the i^{th} amino acid in the test sample, μg/ml;

$X_{standard,\,i}$: Concentration of the i^{th} amino acid standard, μg/ml;

$Y_{sample,\,i}$: Area of the test sample (adjusted by the internal standard);

$Y_{standard,\,i}$: Area of the i^{th} amino acid (adjusted by the internal standard);

$B_{adj,\,i}$ Interception of the established calibration curve using the i^{th} amine acid standard;

$K_{adj,\,i}$ Slope of the established calibration curve using the i^{th} amine acid standard.

i, Alanine, Glycine, Valine, Leucine, Isoleucine, Threonine, Proline, Aspartic acid, Methionine, Glutamic acid, Phenylalanine, Tryptophan, Lysine, and Aspatagine

Linearity of quantification of amino acid standards

Compound	Linear range (µg/ml) [a]	n	corr. coeffs.[b]
Alanine	0.2-35.0	9	0.9992
Glycine	0.2-35.0	9	0.9995
Valine	0.2-35.0	9	0.9992
Leucine	0.2-35.0	9	0.9996
Isoleucine	0.2-35.0	9	0.9993
Threonine	0.2-20.0	8	0.9983
Proline	0.2-35.0	9	0.9985
Aspartic acid	0.2-35.0	9	0.9908
Methionine	0.5-25.0	7	0.9989
Glutamic acid	0.2-25.0	7	0.9981
Phenylalanine	0.5-25.0	7	0.9981
Tryptophan	5.0-35.0	6	0.9907
Lysine	5.0-35.0	6	0.9979
Aspatagine	5.0-35.0	6	0.9990

[a] Each standard stock solution of test compounds was freshly prepared in distilled water (0.8 mg/ml). The mixed standard solution was obtained by adding 100 µl of each stock solution described above. Different volumes of the mixed standard solution were diluted into 600 µl of water for linear range determination. [b] Correlation coefficients were calculated for linearity ranging at the concentration listed here.

1

S2. SUPPORTING FIGURES

SUPPORTING FIG. 1. Typical GC/MS total ion current (TIC) chromatograms of each region of brain tissue samples from the CUMS-treated rats (**(a)** cerebral cortex, **(b)** hippocampus, **(c)** thalamus, and **(d)** the remaining brain regions) and the healthy rats (**(e)** cerebral cortex, **(f)** hippocampus, **(g)** thalamus, and **(h)** the remaining brain regions).

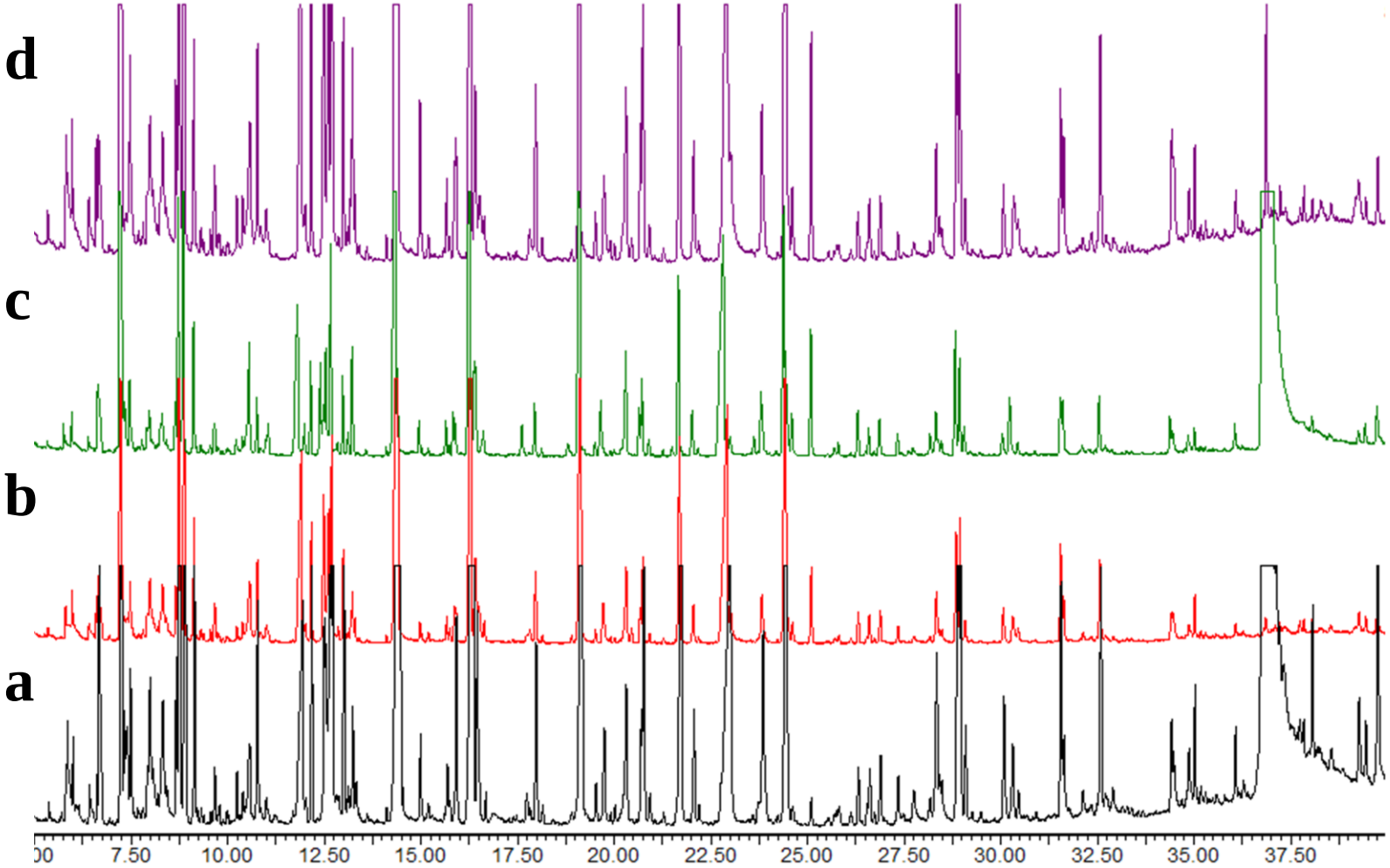

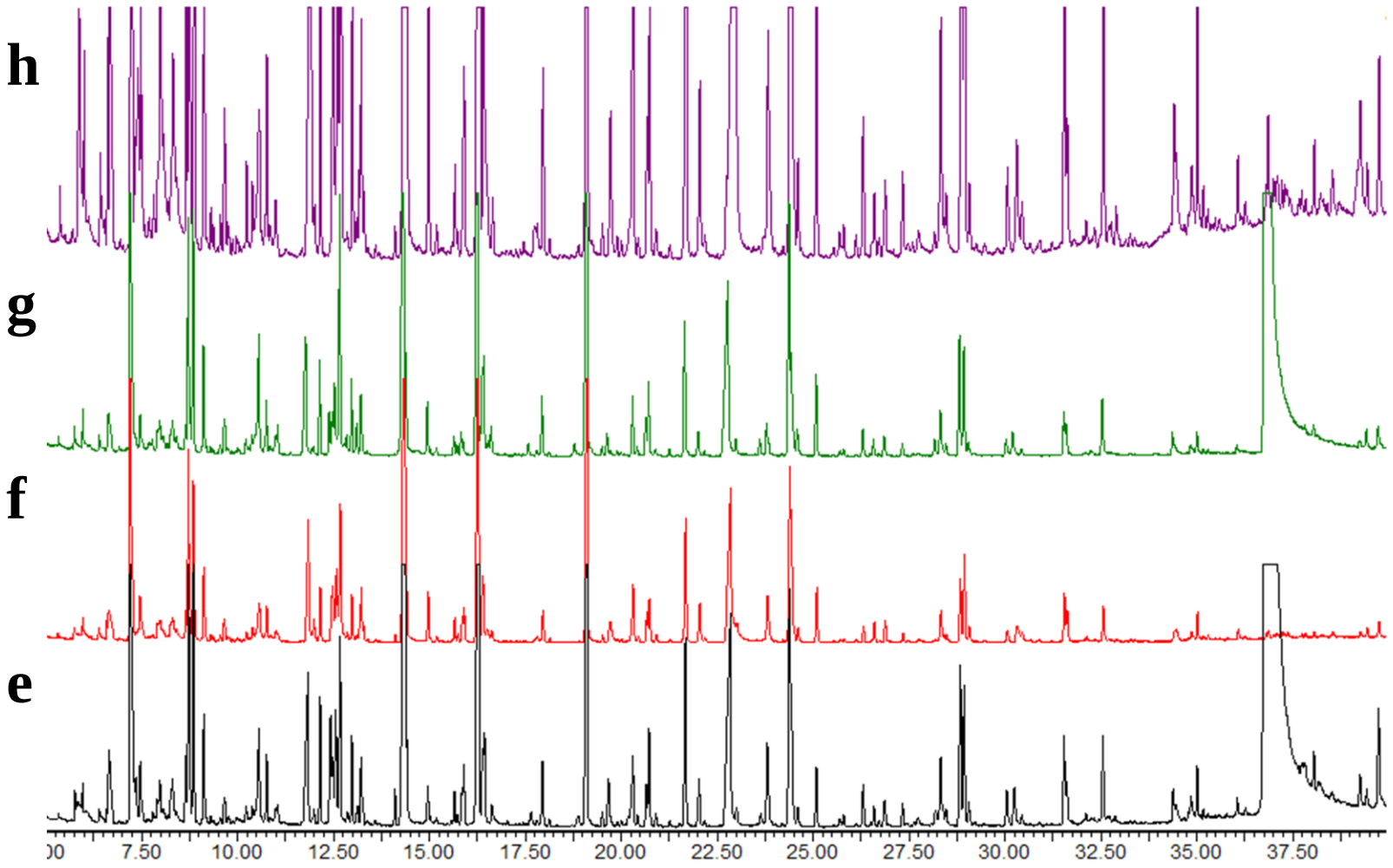
h
g
f
e
)0
7.50
10.00
12.50
15.00
17.50
20.00
22.50
25.00
27.50
30.00
32.50
35.00
37.50

SUPPORTING FIG. 2. 2D-PCA scores map (PC1 *versus* PC2) and 3D-PCA scores map (PC1 *versus* PC2 *versus* PC3) of GC/MS data deriving from the four discrete brain regions of the CUMS-treated group and the healthy control group (n = 6 *per* group).

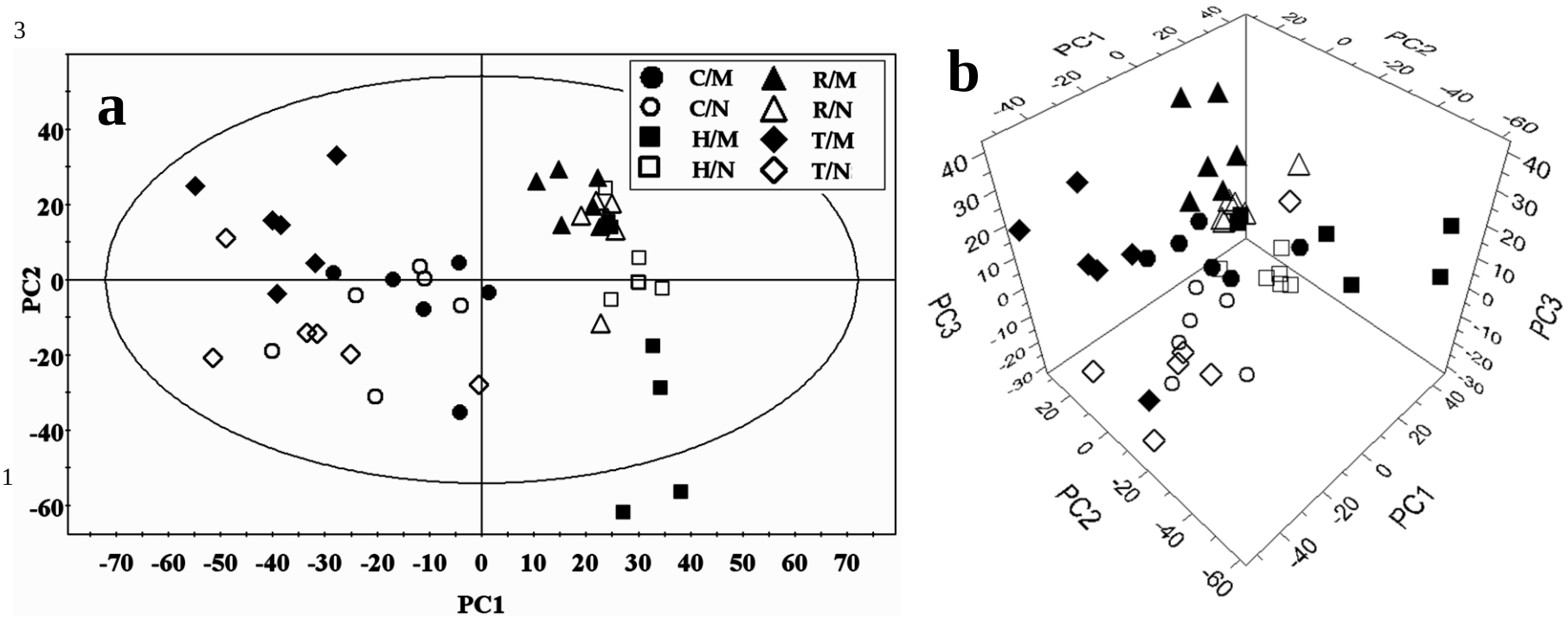

Note: In this study, a five-component PCA model with R2X of 67% was obtained. We only provided the 2D PCA scores plot (PC1 versus PC3) in the TEXT to indicate the inherent differences between brain regions and in relation to stress factors. From this map, we can notice the differences between cerebral cortex or thalamus versus hippocampus or the remaining regions occurred mainly in the PC1 while the consequences of stress are clearly shown in the PC3. The remaining principal components could represent other metabolic differences e.g., PC2 displayed the metabolic differences between thalamus or the remaining regions versus hippocampus (2b), inter-individual differences, and analytical variations etc., therefore, we provided the two additional figures for better understanding of our work.

SUPPORTING FIG. 3. 3D-PCA scores map of GC/MS data deriving from **(a)** hippocampus, **(b)** thalamus, and **(c)** the remaining brain regions obtained from the CUMS-treated group *versus* the healthy control group (n = 6 *per* group). 1D cross-validated OPLS-DA score map of GC/MS data deriving from **(d)** hippocampus, **(e)** thalamus, and **(f)** the remaining brain regions obtained from the CUMS-treated group versus the healthy control group (n = 6 *per* group). The modeled score value (**t[1]p**), the 6th round cross-validated score value (**t[1]cv$_6$**), and orthogonal score value (**t[2]o**) for each individual are illustrated for each observation.

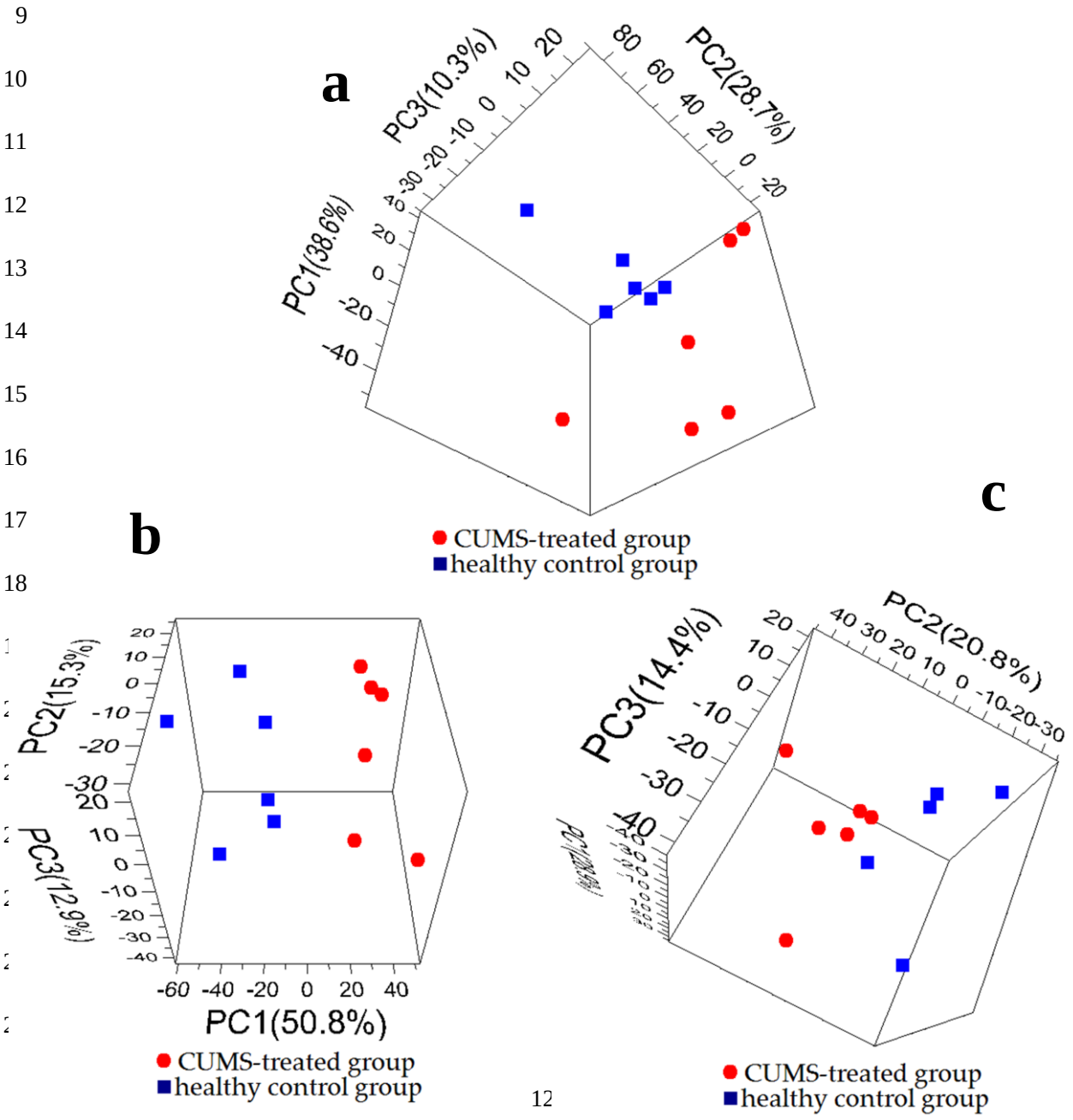

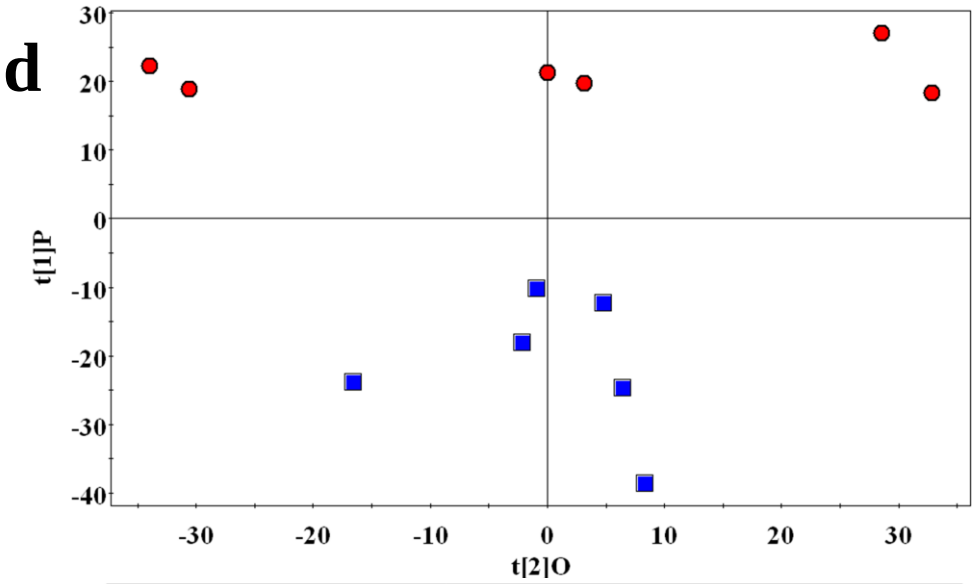
d
30
20
10
0
-10
-20
-30
-40
t[1]P
-30
-20
-10
0
10
20
30
t[2]O

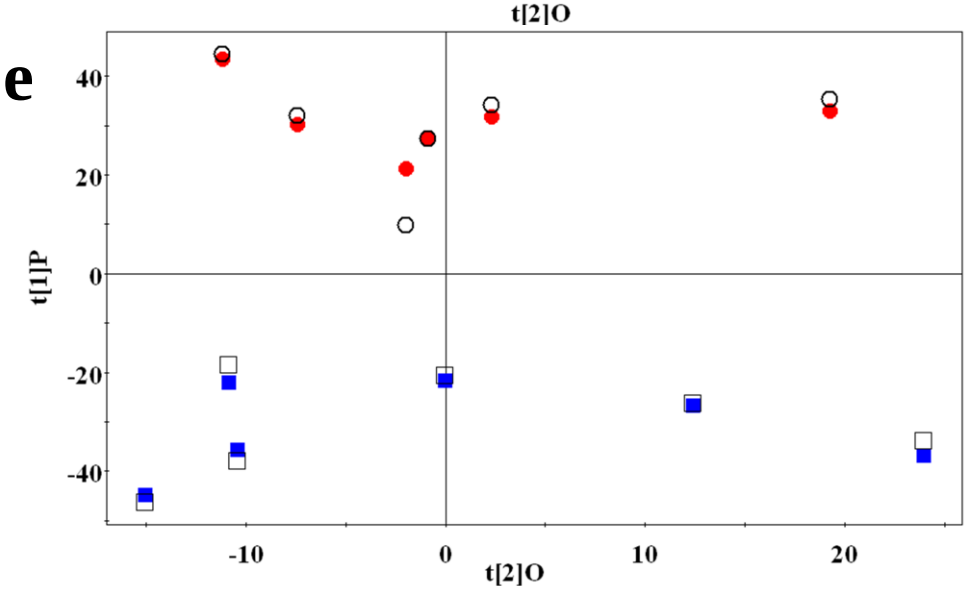
e
40
20
0
-20
-40
t[1]P
-10
0
10
20
t[2]O

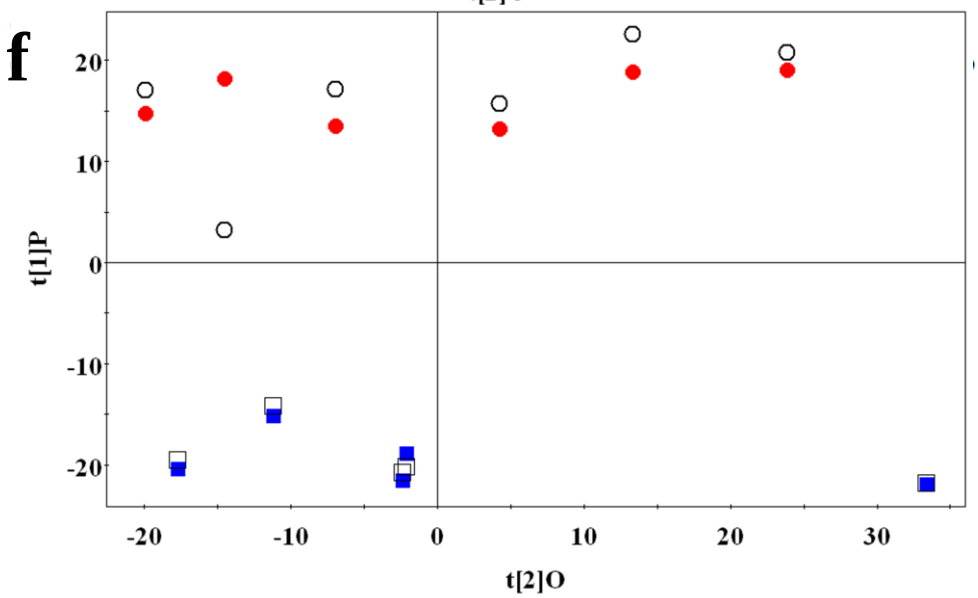
f
20
10
0
-10
-20
t[1]P
-20
-10
0
10
20
30
t[2]O